Available online at www.sciencedirect.com
SCIENCE DIRECT®
Nuclear Instruments and Methods in Physics Research A 510 (2003) 334–345
NUCLEAR INSTRUMENTS & METHODS IN PHYSICS RESEARCH Section A
www.elsevier.com/locate/nima

Test of adiabatic spin flippers for application at pulsed neutron sources

W.H. Kraan[a,*], S.V. Grigoriev[b], M.Th. Rekveldt[a], H. Fredrikze[a], C.F. de Vroege[a], J. Plomp[a]

[a] *Interfacultair Reactor Instituut, TUDelft, Mekelweg 15, 2629 JB Delft, The Netherlands*
[b] *Petersburg Nuclear Physics Institute, 188350 Gatchina, Russia*

Received 17 December 2002; received in revised form 10 April 2003; accepted 15 May 2003

Abstract

Experimental results on the flipping efficiency are shown for a set of 2 V-coils as spin flipper and for a high-frequency flipper with adiabatic transition. The influence of the adiabaticity parameter is discussed. The merits of these adiabatic flippers are compared with the use of "monochromatic" flippers, when operated in a beam from a pulsed neutron source. It is concluded that for "long pulse" sources adiabatic flippers will be superior.

PACS: 07.55.−w; 29.25.Dz; 29.27.Hj; 29.27.Eg

Keywords: Polarised neutrons; Spin flipper; Adiabaticity parameter; Pulsed source

1. Introduction

Spin flippers are essential components in set-ups using polarised neutrons. To take full advantage of a pulsed neutron source flippers must have a good efficiency over the full thermal spectrum. Flippers based on various principles (e.g. resonance [1], Larmor precession in some magnetic field configuration [2,3]) operate over a limited wavelength-band. By proper design parameters this band can be extended, sometimes at the expense of including wavelengths with non-full flipping efficiency. In principle, such flippers are monochromatic. Alternative types of flipper work over the full thermal spectrum. An example is the high-frequency flipper with static gradient field [4] using the principle of adiabatic rotation of the polarisation vector of the neutron beam from the initial to the opposite direction. Another example has a static field, changing sign gradually over a finite beam path length [5].

By flipping we do not understand a geometrical inversion of the orientation of the neutron polarisation, but an inversion relative to the local magnetic field, or mirroring about the plane perpendicular to the field. Hence a device in which the field together with the polarisation rotate as a screw over π over some beam path length, is not a flipper.

In the flipping process the beam might be depolarised, in other words, the efficiency of

*Corresponding author. Fax: +31-15-786422.
E-mail address: kraan@iri.tudelft.nl (W.H. Kraan).

0168-9002/03/$ - see front matter
doi:10.1016/S0168-9002(03)01812-6

flipping might be less than 1. The polarisation of a beam with initial polarisation P_0 after a flipper of efficiency ε is converted to $P_1 = (1-2\varepsilon)P_0$, hence:

$$\varepsilon = (-P_1/P_0 + 1)/2. \quad (1)$$

After two flippers P_2 is again parallel to P_0, so $\varepsilon_1\varepsilon_2 = (P_2/P_0 + 1)/2$.

The behaviour of the polarisation vector **P** in a flipper is determined by the precession equation: $d\mathbf{P}/dt = (\mu_n/\hbar)[\mathbf{P}\times\mathbf{B}]$, where **B** is the magnetic induction and μ_n is the neutron's magnetic moment. Its solution is the well-known rolling of the vector **P** over a cone with axis **B**. If **B** depends on position along the beam axis—i.e. on time as seen in the frame moving with the neutron—the solution is characterised by the adiabaticity parameter k, which is equal to the local Larmor precession frequency $\omega_L = \mu_n|B|/\hbar$, divided by the rotation frequency $\omega_{geo} = v|d\alpha/dx|$ of the field as in the frame moving with the neutron (where the neutron moves at velocity $v = h/(m\lambda)$ in the x direction, and α is the angle between the z-axis and the resultant field at any position along the beam):

$$k = \frac{2\pi\mu_n m|B|}{h^2|d\alpha/dx|}\lambda. \quad (2)$$

Two limiting cases are evident immediately: (i) $\omega_L \gg \omega_{geo}$, i.e. $k\to\infty$. The axis of the precession cone "follows" the vector **B**, hence no flip occurs ("adiabatically following"); (ii) $\omega_L \ll \omega_{geo}$, i.e. $k\to 0$. The axis of the precession cone does not follow **B** at all, so spin flip occurs.

For k between 0 and ∞, the solution of the precession equation for a field transition in the shape of a uniform screw over half a turn can be found in the literature (e.g. Robiscoe [7]). ε is given by:

$$\varepsilon = 1 - \frac{\sin^2((\pi/2)\sqrt{1+k^2})}{k^2+1}. \quad (3)$$

In this article we discuss two types of adiabatic flippers. The first is a set of 2 V-coils (see Fig. 1), as developed in Delft 10 years ago [8]. In fact, this flipper was a byproduct of polarisation rotators for 3D polarisation analysis applicable for the full "white" neutron spectrum. In these rotators a $\pi/2$ turn of the polarisation vector is produced. V-coils can also be used in a spin-echo set-up to orient the

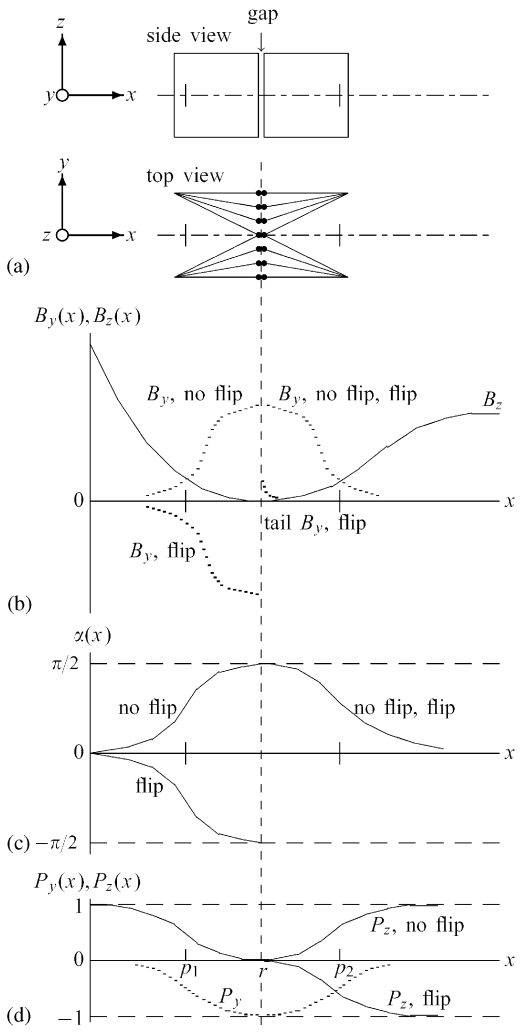

Fig. 1. (a) Side and top views of a flipper made of two V-coils, positioned between a polariser magnetised along z and a guide field $\|z$ (b) Schematic plots of the y and z components of the resulting field in the V-coils; (c) its angle α toward the z-axis and (d) the polarisation components P_y (dotted line) and P_z (full line) along the beam line (x-axis).

polarisation perpendicular to the precession field ($\pi/2$-flipper). A very similar type of flipper was built by Takeda et al. [9].

The second type is the longitudinal high-frequency (HF) coil inside a static gradient field mentioned above (Fig. 5), proposed already in 1975 in Dubna [10] and developed in Gatchina [4]. At present such flippers are applied at many places

(e.g. see Ref. [6]). For application at high fields we extended this type to frequencies up to 2 MHz [11–13]. As a matter of fact, to test this HF flipper, we used V-coils as π- and as $\pi/2$ flipper.

For both types we present data for ε as a function of wavelength, combined with an analysis of the parameter k as derived from field measurements along the beam. Contrary to Weinfurter and Badurek [14] who gave an analytical ansatz to improve ε by properly shaping the fields inside the flipper, we add some field around the position along the beam where k is minimum. We will demonstrate the improvement in efficiency. We point out that ε for a V-coil flipper is in principle smaller than 1, in both modes flip and non-flip; the HF flipper, however, has $\varepsilon = 1$ in the mode flip.

In the last section we compare the efficiency of these adiabatic flippers with the efficiency of a "monochromatic" flipper, installed in a beam from a pulsed source. This flipper is tuned in time such that it remains optimised ($\varepsilon \simeq 1$) for all successive time channels [15,16]. With the advent of "long pulse" sources, the pulse duration can be so long that a neutron spectrum of finite width is present in the flipper at any time. We will see that this spectrum, moreover, gets wider as the flipper is positioned closer to the source. Therefore, optimal tuning of the flipper will become problematic. Eventually, an adiabatic flipper will have better overall efficiency.

2. V-coils as flipper

This flipper is a set of 2 V-shaped coils (dimensions $15 \times 15 \times 15\ \mathrm{cm}^3$) inside a magnetic shielding to provide a path without magnetic resistance for the return flux. Fig. 1a gives a top and a side view. At $x = r$ (dashed line) are 2 screens of parallel wires, traversed by the neutrons. Each coil produces a horizontal field terminated at the screen position.

In the mode "flip" (f) the fields in the V-coils are $\| -y$ and $+y$, successively. Between the polariser and the first V-coil the polarisation follows the local field adiabatically from z (direction stray field polariser) to $-y$ (field direction deep inside the first V-coil). At $x = r$ the polarisation does not follow the field reversal (field second V-coil $\| +y$), so beyond $x = r$ it is anti-parallel to the local field. In this relative orientation it follows the local resultant field adiabatically over the length between the second V-coil (field $\|y$) and the guide field ($\|z$), hence the polarisation ends in the "flipped" state.

In the mode "no flip" (n) the field in the first V-coil is switched parallel to the second (y) and no spin flip occurs at $x = r$.

The components of the field are plotted in Fig. 1b; they suggest that the absolute value of the resulting field is minimum at $x = p_1$ and p_2 where $B_y = B_z$. The angle $\alpha(x)$ between the local resulting field and the z-axis is given in Fig. 1c, showing that $\mathrm{d}\alpha(x)/\mathrm{d}x$ will be maximum in these points. Hence, the parameter k will be minimum at these positions. These minima effectively determine the quality of the flipper.

2.1. Test method of this flipper

For testing, a time-of-flight (TOF) set-up with 2 identical V-coil flippers was built (Fig. 2), between a polariser and an analyser which are anti-parallel to each other. The field transitions T1–T4 in front of and behind the flippers F1 and F2 are characterised for both modes (flip (f), no flip (n)) of both flippers. TOF spectra I_{nn}, I_{nf}, I_{fn} and I_{ff} were taken in all modes. In the modes nn and ff (0,2 flips) the neutron spin just beyond r_2 has the same orientation as just in front of r_1. From this orientation it rotates adiabatically in region T4 to the orientation of the analyser, hence the spectra I_{nn} and I_{ff} are "light" (high intensity). The other spectra involve one flip, so the spin beyond r_2 is opposite to the previous case; these spectra are "dark".

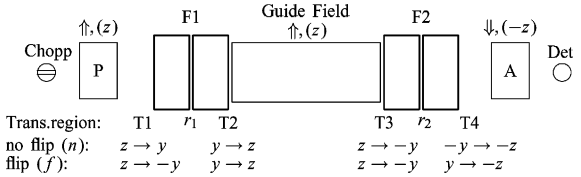

Fig. 2. Side view of test set-up.

The problem of analysing such a set of spectra has been treated by several authors, e.g. Wildes [18]. We follow the analysis by Fredrikze and van de Kruijs [19] who give equations for the intensities $I^0_{pp}, I^0_{aa}, I^0_{pa}$ and I^0_{ap} measured in a neutron reflectometer with polarisation facility, for the case without sample. In Ref. [19] the indices p and a refer to a fixed orientation in space, both at the polariser and analyser sides of the sample position. In our case the first index p/a (referring in Ref. [19] to the polariser side; here to F1) becomes n/f, respectively. Because our analyser is anti-parallel to the polariser, the second index p/a (analyser side; F2) becomes f/n, respectively.

Each flipper will depolarise the beam. The full depolarisation in mode nn is accounted for by a factor Q. As pointed out in the Introduction, V-coil flippers will give depolarisation in both modes. Following [19] we assume that the depolarisation D_n per flipper in mode n might differ from the depolarisation D_f in mode f, by introducing the factors $\rho = D_n/D_f$ for flipper F1 and $\alpha = D_n/D_f$ for flipper F2. So, the full depolarisation factors for the modes nn, nf, fn and ff become Q, αQ, ρQ and $\alpha\rho Q$, respectively. Then, the equations for I_{nn}, I_{nf}, I_{fn} and I_{ff} (corresponding to I^0_{pa}, I^0_{pp}, I^0_{aa} and I^0_{ap} in Ref. [19]) become

$$I_{nn} = (I_0/2)(1 + \Pi_p\Pi_a Q) \tag{4}$$

$$I_{nf} = (I_0/2)(1 - \Pi_p\Pi_a\alpha Q) \tag{5}$$

$$I_{fn} = (I_0/2)(1 - \Pi_p\Pi_a\rho Q) \tag{6}$$

$$I_{ff} = (I_0/2)(1 + \Pi_p\Pi_a\alpha\rho Q) \tag{7}$$

where $\Pi_p\Pi_a$ is the product of the intrinsic polarising efficiencies Π_p and Π_a of the polariser and analyser. These equations contain I_0, α, ρ and the product $\Pi_p\Pi_a$ as unknowns which can be solved. The solution reads

$$I_0 \text{ (net spectrum)} = 2\frac{I_{ff}I_{nn} - I_{nf}I_{fn}}{I_{nn} + I_{ff} - I_{fn} - I_{nf}} \tag{8}$$

$$\Pi_p\Pi_a\, Q \text{ (depolarisation)} = \frac{(I_{nn} - I_{fn})(I_{nn} - I_{nf})}{I_{nn}I_{ff} - I_{nf}I_{nf}} \tag{9}$$

$$\rho \text{ (asymmetry F1)} = \frac{I_{ff} - I_{fn}}{I_{nn} - I_{nf}} \tag{10}$$

$$\alpha \text{ (asymmetry F2)} = \frac{I_{ff} - I_{nf}}{I_{nn} - I_{fn}}. \tag{11}$$

2.2. Results: polarisation of an empty beam

To separate the depolarisation Q due to the flippers from the product $\Pi_p\Pi_a$ calculated according to Eq. (9), we need to find the product of the polarising efficiencies Π_p and Π_a. To find this product, we removed both flippers, so the set-up consisted only of the polariser and the anti-parallel analyser. Their stray fields were extended until halfway between. We measured the TOF spectra "I_{min}" (with halfway a field step device containing antiparallel V-coils) and "I_{plus}" (with halfway a device in which the magnetic induction (5 mT) rotates uniformly over 180° over 0.3 m; the parameter k for 0.1 nm of this device equals 180, so the polarisation follows adiabatically). The polarisation:

$$P_0 = (I_{plus} - I_{min})/(I_{plus} + I_{min}) \tag{12}$$

is plotted in Fig. 3 as a function of TOF channel (i.e. λ) as a bold line.

Another way of finding $\Pi_p\Pi_a$ is to multiply the data of the net polarising efficiencies of polariser and analyser as determined by means of the 3P2F method [17] in earlier TOF experiments with the explicit purpose of determining Π_p and Π_a of the same polarisers [20]. The product $\Pi_p\Pi_a$ found in this way is plotted in Fig. 3a as a dotted line. (The irregularity around $\lambda = 0.8$ nm is from noise pulses of the chopper. The discrepancy below $\lambda = 0.2$ nm is due to a lack of intensity in the set-up for the 3P2F method: it contains three instead of two polarisers having transmissions approaching 0 at low wavelength.)

In the 3P2F method (published in Ref. [17] as "3P2S" method) three polarisers P, X and R are aligned in a beam, their magnetic directions being chosen at convenience. P, X and R could be all of different constructions. Flippers (in Ref. [17] shims) installed in the gaps P–X and X–R are each operated in both modes, giving four intensities with the polarising efficiencies Π_p, Π_x, Π_r and the "intrinsic" intensity as unknowns. The solution for Π_p and Π_r includes the full

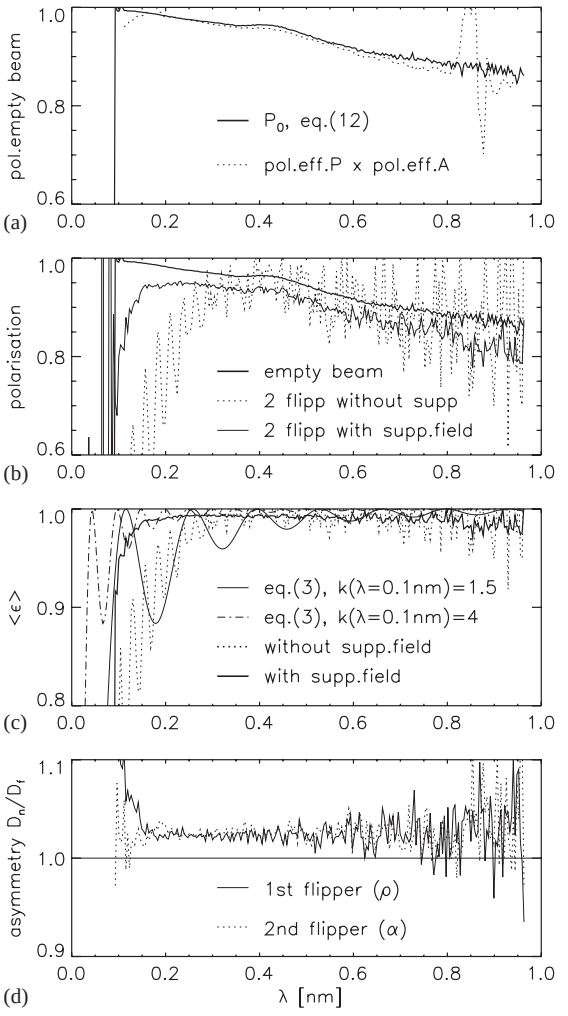

Fig. 3. V-coil flipper: (a) polarisation empty beam without flippers and as imposed by the efficiency Π_p and Π_a of the polarisers; (b) effective polarisation with both flippers in mode n; (c) average efficiency $\langle\varepsilon\rangle$ per flipper, found using Eq. (1) after dividing the effective polarisation (b) by the empty beam polarisation (a). Also shown: $\langle\varepsilon\rangle$ according to Eq. (3), with adiabaticity parameter $k(\lambda = 0.1\ \text{nm})$ chosen to be 1.5 and 4; (d) asymmetry between n and f (Eqs. (10), (11)), with support field.

depolarisation (including flippers) in the gaps P–X and X–R, respectively. The result Π_x—efficiency polariser being tested—includes no depolarisation.

Fig. 3a shows that P_0 is indeed equal to the product $\Pi_p\Pi_a$ of the intrinsic polarising powers of the polarisers to within 1%. This means that the product $\Pi_p\Pi_a$ can be reliably divided out of the result for Eq. (9), hence the value found for Q can be attributed to the flippers.

2.3. Efficiency flippers in mode n

The result for $\Pi_p\Pi_a$ Q (Eq. (9)) with the flippers in their initial shape, is given as the dotted line in Fig. 3b (beam cross-section $10 \times 30\ \text{mm}^2$). Division by $\Pi_p\Pi_a$ (Fig. 3a, full line) gives Q, the depolarisation due to two identical flippers in mode nn. Identifying $Q \equiv P_2/P_0$ (Eq. (1)) gives the average efficiency $\langle\varepsilon\rangle$ per flipper for mode n. It is plotted as the dotted line in Fig. 3c. We see that $\langle\varepsilon\rangle$ rises in an oscillating way, approaching 1 at $\lambda \simeq 0.4$ nm.

2.4. Adiabaticity parameter

These oscillations can be qualitatively understood from the behaviour of ε predicted by Eq. (3). In Fig. 3c, ε is plotted for k chosen to be 1.5 and 4 for $\lambda = 0.1$ nm. By comparing the decrease and periodicity in ε as measured with this prediction, it can be only said that $k(\lambda = 0.1\ \text{nm})$ ranges between 1 and 10. The failure to give a quantitative description of $\langle\varepsilon\rangle$ as a function of λ is due to the fact that the fields in the regions T1–T4 do not rotate uniformly, as assumed in Eq. (3).

Fig. 4 shows how this was analysed. Fig. 4a gives the field profiles of flipper F1, measured in its initial configuration. Fig. 4b contains the angle α and its derivative needed to calculate ω_{geo} using Eq. (2); Fig. 4d gives the result, together with ω_L found from $|B|$, plotted in Fig. 4a. The bold lines without symbols in Fig. 4d give the adiabaticity parameter k. Near the points $x = r_1$ and r_2 characterised in Fig. 1 k drops nearly to 1.

The left minimum was raised by adding some z-field ("support field") by means of permanent magnets. The resulting field profiles for F1 are shown in Fig. 4c. The parameter k after this modification is given in Fig. 4d by the bold line with symbols. (F2 was improved in an analogous manner). $\Pi_p\Pi_a Q$ and $\langle\varepsilon\rangle$ measured after this modification are plotted as full lines in Figs. 3b

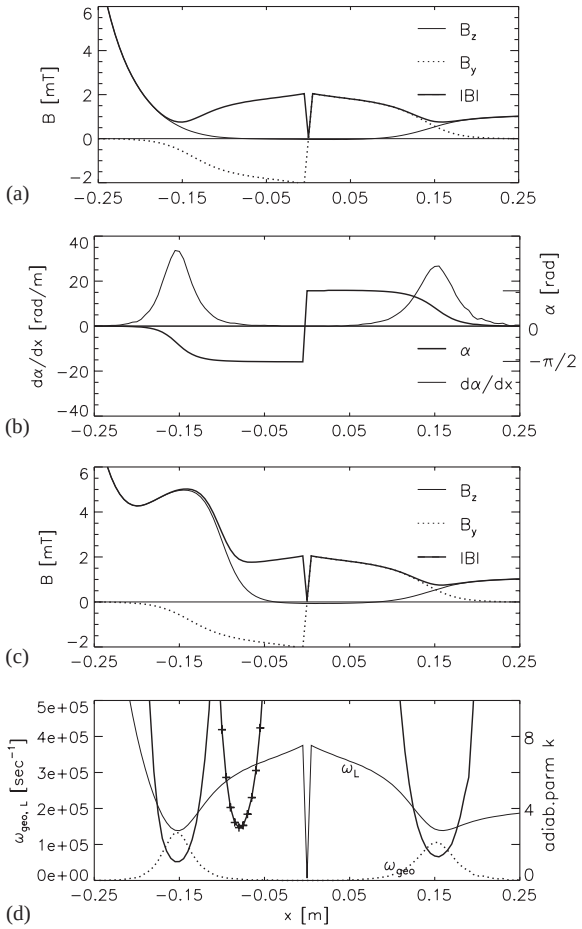

Fig. 4. V-coil flipper: (a) Measured field profiles without support field; (b) angle $\alpha(x)$ between resulting field and z-axis (scale to the right) and $d\alpha/dx$; (c) Field profiles after improvement with support field. (d) Larmor frequency ω_L (from $|B|$) and "geometrical" frequency ω_{geo} (from $d\alpha/dx$, for $\lambda = 0.1$ nm) as initially, without support field. Bold lines (without/with symbols): adiabaticity parameter k for the configurations (without/with) support field (scale to the right).

and c (beam cross-section 30×30 mm^2). For λ as low as 0.15 nm $\langle \varepsilon \rangle$ appears to approach 1.

For an account of this result using Eq. (3), we should take $k(\lambda = 0.1$ nm) to be at least 10. The period in the oscillations becomes so small that it damps out in view of the wavelength resolution of our TOF set-up.

If space around the beam permits, other ways to improve k would be: to position the flipper properly in the stray fields of the adjacent devices or to increase the dimensions of the flipper perpendicular to the beam. This will make the positioning of the flipper less critical.

2.5. Asymmetry between n and f

Fig. 3c gives the asymmetries ρ and α for flippers F1 and F2 after the modification. The asymmetry might have two origins.

Firstly, the z-fields from the polariser and the guide field around F1 in principle extend beyond its mid-point $x = r$. As a consequence, the polarisation vector just before $x = r$ has some z-component which is transferred into the second V-coil together with the y-component. This means that in mode f the flip at $x = r$ is not exact. For mode n it has no consequences.

Secondly, the field of the V-coils does not end exactly at $x = r$, but has some negative tail beyond this point (Fig. 1b: "tail B_y, flip"). In mode f the tails produced by the two adjacent V-coils largely cancel each other, but in the mode n they add, so in the gap (1 mm) between the coils (see Fig. 1a) a y-field of the order 2 mT exists. The polarisation which already has some z-component by the previous effect, precesses in this gap over an angle amounting in the worst estimation to $\simeq 0.3$ rad for $\lambda = 0.5$ nm. This precession, occurring only in mode f, might explain why ρ and α are both greater than 1. (The data for the initial state of the flippers without support field are too poor to see the asymmetry.)

3. Adiabatic HF flipper with gradient field

The second type of flipper is an "HF flipper with adiabatic transition", shown in Fig. 5. It consists of a longitudinal high-frequency (HF) coil (length 60 mm, diameter 30 mm, 19 windings) in a static transversal field, composed of a "homogeneous" contribution B_0 and a static gradient field. Two capacitors could be switched parallel to the HF coil, giving resonance at 1.08 and 2.25 MHz. The frequency must be chosen such that at some point inside the coil, it corresponds to the Larmor frequency $\omega_0 = \mu_n B_0/\hbar$ of the resulting static field.

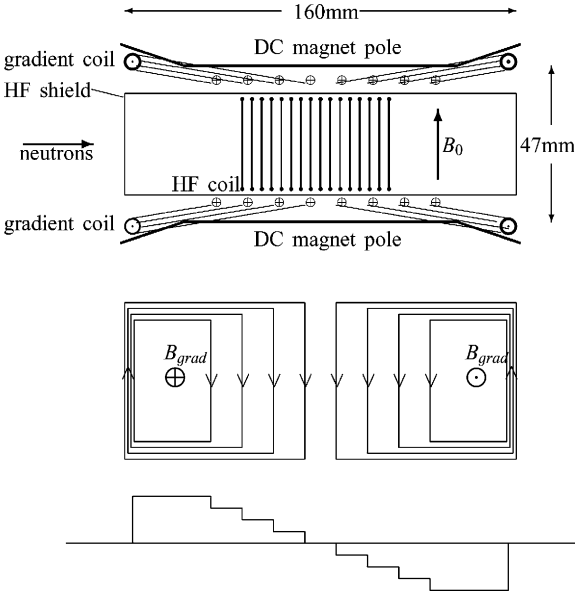

Fig. 5. Side view of an adiabatic HF flipper and top view of the windings generating the gradient field, which is shown schematically in the bottom profile.

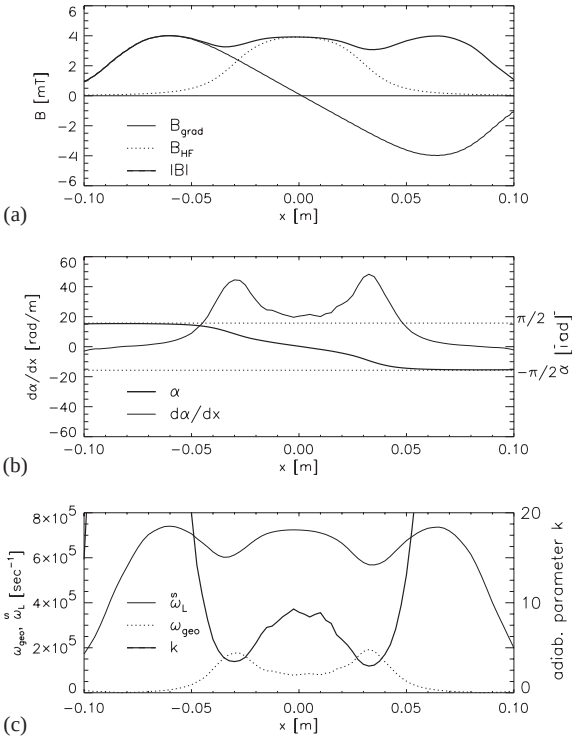

Fig. 6. Adiabatic HF flipper: (a) Profiles of the DC-gradient field (measured with the DC-current adjusted for 4 mT amplitude), of the HF field (calculated analytically for a current such that max = 4 mT) and of the absolute value of the resulting field; (b) angle α and $d\alpha/dx$ of the resulting field toward xy-plane; (c) $\tilde{\omega}_L$ (from $|B|$) and ω_{geom} (from $d\alpha/dx$) and adiabaticity parameter (scale to the right).

Therefore the static field B_0 was set to 36 and 77 mT, respectively. It is generated by an electromagnet; the gradient field is produced by the extra windings against the poles shown in Fig. 5. Fig. 6a shows the measured field profile, for a current chosen such that the maximum field (denoted gradient amplitude A_{grad}) equals 4 mT. The field profile of the HF coil was calculated analytically (dotted line in Fig. 6a) for a current such that its maximum A_{HF} also equals 4 mT. In practice A_{HF} was measured and set by means of a pick-up coil placed at the position of the maximum.

The behaviour of the neutron spin in the combined magnetic fields is explained in several papers mentioned above, e.g. Refs. [4] and [6]. It can be understood in a coordinate system $(\tilde{x}, \tilde{y}, z)$ rotating around the direction of the static field at the frequency ω_0 imposed on the HF coil. In this system the field B_0 is "transformed away", hence only the gradient field remains as a static field parallel to z. If we imagine an HF field component along y, shifted by $\pi/2$ with respect to the existing HF field, we have an HF field rotating at ω_0 around z. In the system $(\tilde{x}, \tilde{y}, z)$ it has a fixed orientation in the $\tilde{x}\tilde{y}$-plane. The phase angle of this field (denoted $\tilde{B}_x$) can be chosen such that it is parallel to $\tilde{x}$. The plots in Fig. 6a can be considered to represent the remaining gradient field and the field $\tilde{B}_x$. The absolute value of this field determines a Larmor frequency $\tilde{\omega}_L = \mu_n \sqrt{\tilde{B}_x^2 + B_{grad}^2}$, plotted in Fig. 6c as a full thin line. The neutrons, when moving through this field configuration, experience a field rotating in the $\tilde{x}z$-plane from $+z$ to $-z$. Its angle $\alpha = \arctan(B_{grad}/B_{HF})$ toward the $\tilde{x}\tilde{y}$-plane and $d\alpha/dx$ are plotted in Fig. 6b. The derivative $d\alpha/dx$ translates itself through the neutron velocity into the "geometrical" frequency ω_{geo} of the resulting field, plotted for $\lambda = 0.1$ nm as the dotted line in Fig. 6c. Dividing $\tilde{\omega}_L$ by ω_{geo}

gives the adiabaticity parameter k according to Eq. (2), plotted for $\lambda = 0.1$ nm in Fig. 6c as a bold line. Ref. [11] contains a quantitative solution of the precession in this field configuration for idealised field profiles $B_{\text{grad}} = A_{\text{grad}} \sin(\tilde{x}/l)2\pi$ and $B_{\text{HF}} = A_{\text{HF}} \cos(\tilde{x}/l)2\pi$ (where l is the length of HF coil; the origin of the system $(\tilde{x}, \tilde{y}, z)$ is at its centre).

3.1. Measuring $\varepsilon(A_{\text{HF}}, A_{\text{grad}})$ at $\lambda = 0.22$ nm

To measure the efficiency $\varepsilon(A_{\text{HF}}, A_{\text{grad}})$ of one flipper, four such flippers were installed between the polariser and analyser of the instrument "SP" for 3D polarisation analysis (different from the test set-up for the V-coil flipper). This instrument lacks the TOF facility, but has a pyrolytic graphite crystal (see Fig. 7a) to make monochromatic analysis possible. In front of the analyser a V-coil flipper was installed. To calculate the polarisation of the beam, detector intensities in both modes of this flipper were measured. First, the polarisation P_0 was measured with all the flippers switched off.

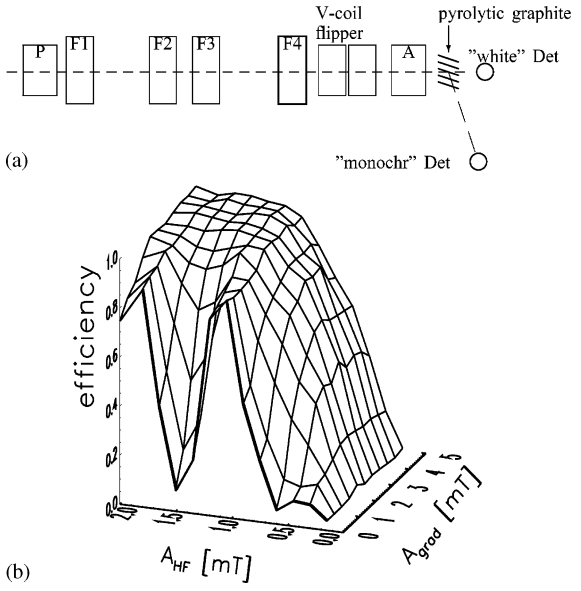

Fig. 7. Adiabatic HF flipper: (a) set-up for measuring the flipping efficiency $\langle \varepsilon \rangle$ in F4, for a monochromatic beam, $\lambda = 0.22$ nm. (b) $\langle \varepsilon \rangle$ measured for HF = 1.08 MHz, $B_0 = 37$ mT as a function of the amplitudes A_{HF} and A_{grad} of the HF and gradient field.

After one HF flipper (F4, Fig. 7a) was switched on, the polarisation P_1 was measured with various settings of A_{HF} and A_{grad}. The efficiency of this flipper, calculated according to Eq. (1) for the signals of the monochromatic detector for $\lambda = 0.22$ nm, is shown in Fig. 7b.

It is unnecessary to calibrate the efficiency of the V-coil flipper because it cancels in the numerator and denominator. The need to separate the empty beam polarisation, as in testing the V-coil flipper, does not arise here, because it is identical to P_0 measured in mode non-flip (n) where depolarisation is absent.

Fig. 7b illustrates the transition from a "resonance flipper" to an adiabatic HF flipper, as the gradient amplitude A_{grad} increases from 0. In the resonance mode ($A_{\text{grad}} = 0$) the period in the efficiency corresponds to an amplitude A_{HF} such that $(\gamma_N/h) \int B_{\text{HF}}(\tilde{x})\, \mathrm{d}\tilde{x} \simeq (\gamma_N/h) A_{\text{HF}} l/2 = \pi$. This periodicity is confirmed. The irregularity in period for $A_{\text{grad}} \to 0$ is due to the inhomogeneity of the field B_0 and a threshold in the output of the HF generator used to trigger the circuit containing the HF coil.

3.2. Measuring $\varepsilon(\lambda)$

To measure the efficiency as a function of λ, we used a Fourier method [21]. To do this, the set-up of Fig. 7a was modified to the configuration of Fig. 8a. The $\pi/2$ flippers (V-coils) cause the polarisation vector to precess around the static fields B_0 inside and around the flippers. By switching the static fields of F1 and F2 anti-parallel to those of F3 and F4, the set-up operates in the spin echo mode. The induction B inside the coil between flippers F2 and F3 is varied in order to offset the set-up around the echo condition. As a consequence, for any wavelength the intensity $I(B)$ in the detector behind the analyser **A** will oscillate as a function of B. All wavelengths in the neutron spectrum together give (after subtracting the average intensity I_s):

$$I(B) - I_s \equiv I(c^* B) - I_s = \int_0^\infty F(\lambda) \cos(c^* \lambda B)\, \mathrm{d}\lambda,$$

which is the cosine Fourier transform of the quantity $F(\lambda)$, being the product of the spectral

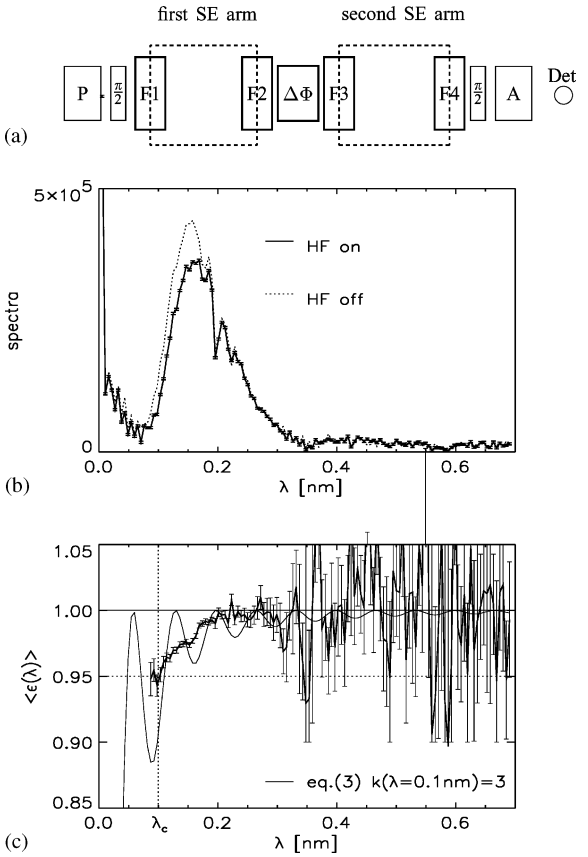

Fig. 8. Adiabatic HF flipper: (a) Spin echo set-up for simultaneous test of 4 flippers. (b) Spectra obtained using Eq. (13) for HF = 1.08 MHz. The dip at 0.2 nm is due to the Al (2 0 0) Bragg cutoff of the windings of the coil $\Delta\Phi$. (c) average efficiency per flipper $\langle\varepsilon\rangle$. Dotted straight lines: illustrating λ_c for minimum efficiency equal to 0.95.

density and the effective polarisation as a function of λ. (The value of the constant c^* connecting the variables λ and B is determined by the construction of the coil "$\Delta\Phi$". It can be calculated from the period in B measured for a monochromatic beam). Upon performing the inverse transformation we obtain $F(\lambda)$ itself:

$$F(\lambda) = \int_{-B_{\max}}^{+B_{\max}} [I(B) - I_s \cos(c^*\lambda B)]\, \mathrm{d}(c^* B). \qquad (13)$$

Measurements taken with flippers off or on ($A_{\mathrm{grad}} = 5$ mT; $A_{\mathrm{HF}} = 2$ mT) yield F_n and F_f, given in Fig. 8b as a function of wavelength. Applying Eq. (1), we have for any λ:

$$\frac{F_f}{F_n} = \frac{P_f}{P_n} = -\frac{P_n(1-2\varepsilon)}{P_n}$$

where ε is the result of four independent flippers, supposed to be equal. Therefore we substitute $\varepsilon = \langle\varepsilon\rangle^4$, where $\langle\varepsilon\rangle$ is the efficiency of a single flipper. So

$$\langle\varepsilon\rangle = \sqrt[4]{\frac{F_f/F_n + 1}{2}}.$$

(The spectral density of the beam and the efficiency of the $\pi/2$ flippers cancel in this calculation). The result as a function of λ for 1.08 MHz is given in Fig. 8c, for a beam of cross-section 5×5 mm^2. We notice, in analogy with Fig. 3, that $\langle\varepsilon\rangle$ starting from 0.1 nm increases quickly to 1, because the adiabaticity parameter k increases with wavelength. To illustrate this, $\langle\varepsilon\rangle$ as expected according to Eq. (3) with the assumption $k(\lambda = 0.1\ \mathrm{nm}) = 3$ is also plotted.

We point out that in spite of the inaccuracy of the data in Figs. 3 and 9, the efficiencies of both the V-coil flipper and the HF adiabatic flipper must approach 1 as λ increases, according to Eq. (3), since k is proportional to λ. Hence, it is meaningful to characterise a flipper by its critical wavelength λ_c, defined as the wavelength beyond which its efficiency exceeds a chosen value $\langle\varepsilon_c\rangle$. For example for $\langle\varepsilon_c\rangle = 0.95$, Fig. 8c shows that λ_c equals 0.1 nm.

4. Monochromatic flippers at a pulsed source

We discuss two models of monochromatic flippers: a flat π-rotating coil (Fig. 9a) and a

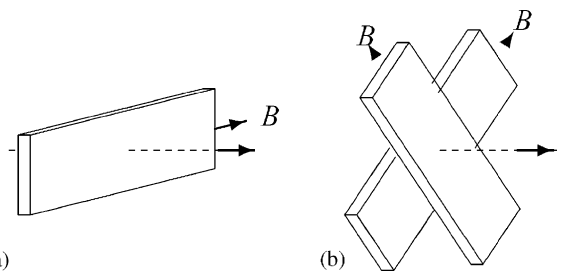

Fig. 9. 2 options for monochromatic flippers.

configuration of two π-rotating flat coils with field at 45° and −45° to the vertical (Fig. 9b). They are embedded in a small homogeneous vertical guide field (negligible compared with the fields inside the flipper), hence, after passage through the flipper the relative orientation between polarisation and local field is reversed. If the fields in the coils are set such that exact flip occurs at wavelength λ_0, it is easily seen that their efficiencies as a function of wavelength are:

$$\varepsilon_{(a)}(\lambda_0,\lambda)=\frac{1}{2}\left[-\cos\left(\frac{\lambda}{\lambda_0}\pi\right)+1\right] \quad \text{(Fig. 9a)} \qquad (14)$$

$$\varepsilon_{(b)}(\lambda_0,\lambda)=\frac{1}{2}\left[-\cos\left(\frac{\lambda}{\lambda_0}\pi\right)+\frac{1}{2}\sin^2\left(\frac{\lambda}{\lambda_0}\pi\right)+1\right] \quad \text{(Fig. 9b).} \qquad (15)$$

These functions are shown in Fig. 10 for two different settings of λ_0. When such a flipper is installed in a neutron beam from a pulsed source, the wavelength λ_0 for optimal flip can be adapted (by properly decreasing the current in the coil) such that ε remains 1 for the neutrons collected in any time channel. Flippers operating according to this principle are installed at ILL [15] and are being developed in Japan by Maruyama et al. [15,16].

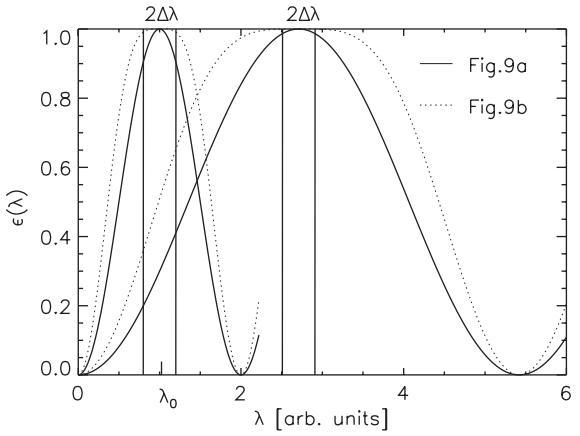

Fig. 10. Efficiency for the monochromatic flippers of Fig. 9. When used in a pulsed beam, the flipper can be tuned such that the argument of the cosine in Eqs. (14) and (15) remains π, hence $\varepsilon \simeq 1$, as neutrons of increasing wavelength pass through (i.e. the interval $2\Delta\lambda$ moves to the right). The flip efficiency $\varepsilon(\lambda)$ is shown for two different time channels ($\equiv \lambda_0$ values).

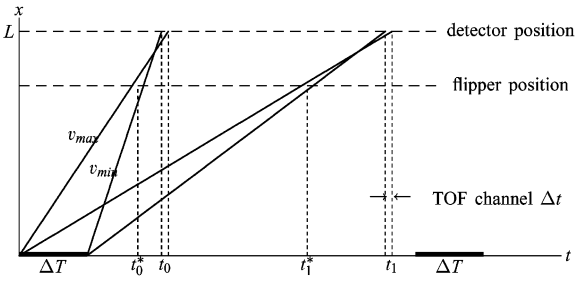

Fig. 11. World diagram of a pulsed neutron beam with a flipper and a detector operated in TOF mode. The beam is assumed to be "on" during the time intervals ΔT and "off" in the remaining time. The thick lines indicate the minimum and maximum neutron velocity at the flipper position in the time channels at t_0 and t_1. (No devices are assumed to affect the time profile of the beam intensity).

However, in any time channel the duration ΔT of the beam pulse gives non-monochromatic neutrons inside the flipper between $v_{\min}$ and $v_{\max}$, indicated in the "world diagram" in Fig. 11 for the time channels at t_0 and t_1. It is seen from this diagram that this velocity interval remains constant in time. In terms of wavelength, its width $2\Delta\lambda$ is

$$2\Delta\lambda=\frac{\Delta T}{L}\frac{h}{m}, \qquad (16)$$

where L is the distance from the source to the detector, h is Planck's constant and m is the neutron mass. The efficiency of the flipper over this interval will be:

$$\langle\varepsilon\rangle(\lambda_0,\Delta\lambda)=\frac{1}{2\Delta\lambda}\int_{\lambda_0-\Delta\lambda}^{\lambda_0+\Delta\lambda}\varepsilon(\lambda_0,\lambda)\,\mathrm{d}\lambda.$$

Fig. 10 illustrates this integration for two different values of λ_0. Upon substituting Eqs. (14) and (15), one obtains (dropping the index $_0$ from λ):

$$\langle\varepsilon_{(a)}\rangle(\lambda,\Delta\lambda)=\frac{1}{2}\left[1+\frac{\sin(A_1(\lambda))}{A_1(\lambda)}\right] \quad \text{(Fig. 9a)}$$

$$\langle\varepsilon_{(b)}\rangle(\lambda,\Delta\lambda)=\frac{1}{2}\left[1+\frac{\sin(A_1(\lambda))}{A_1(\lambda)}+\frac{1}{4}-\frac{1}{4}\frac{\sin(A_2(\lambda))}{A_2(\lambda)}\right] \quad \text{(Fig. 9b)}$$

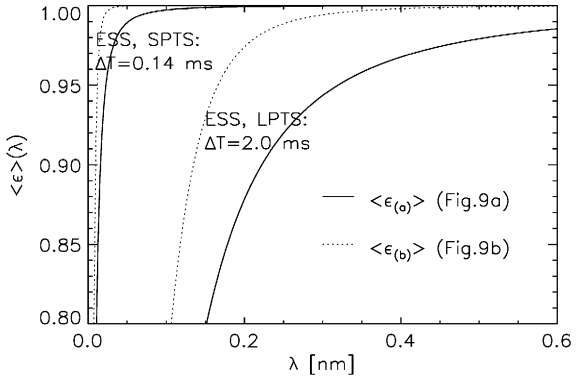

Fig. 12. Efficiencies for the "monochromatic" flippers of Fig. 9, when placed at $L = 10$ m from the "Short Pulse" Target Station (SPTS) and the "Long Pulse" TS (LPTS) at the ESS spallation source. The wavelength interval $2\Delta\lambda$ is determined by Eq. (16).

with

$$A_1(\lambda) = \frac{\Delta\lambda}{\lambda}\pi, \quad A_2(\lambda) = \frac{2\Delta\lambda}{\lambda}\pi$$

and $2\Delta\lambda$ given by Eq. (16).

As an example we take a flipper installed at the projected source ESS at a distance $L = 10$ m from the "short pulse" target station (SPTS, pulse length, incl. decay time 140 μs) and from the "long pulse" target station (LPTS, pulse length 2 ms) [22]. The integration interval $2\Delta\lambda$ for both pulse lengths is found using Eq. (16). The results for $\langle\varepsilon\rangle(\lambda)$ are plotted in Fig. 12.

5. Summary and conclusion

Results for two types of adiabatic spin flippers are presented: V-coils (operating with DC current) and the HF adiabatic flipper with DC gradient field (operating at 1 and 2 MHz).

Results of the flipping efficiency as a function of λ for the V-coil type are presented for the first time. Due to their geometry, the neutron beam must cross two screens of parallel current-carrying wires, at the expense of 1% of intensity. In the mode *non-flip* these screens might produce a net field in the gap between these screens. In the mode *flip* it is absent. Therefore the flip efficiency for this type of flipper is in principle asymmetric. A small asymmetry (1%) was indeed found. It can be reduced by a better magnetic short-circuiting, especially at the position of this gap.

The HF adiabatic flipper has the amplitudes of the HF field and the gradient field as variables. By increasing the gradient field amplitude from zero to some maximum we demonstrate the transition from a "resonance flipper" to an HF adiabatic flipper: the efficiency, initially varying periodically between 0 and 1, rises to 1, for any HF amplitude. The initial period depends on wavelength.

From the definition of the adiabaticity parameter it follows that the efficiency for any flipper goes asymptotically to 1 with increasing wavelength. This is confirmed in our results for both flippers as a function of wavelength. For a chosen efficiency value (e.g. 0.95) a critical wavelength (λ_c) can be found, which is the lower wavelength limit for that efficiency. For a flipper installed in a magnetic surrounding, λ_c is determined by the minimum of the "adiabaticity parameter" along the beam line in and around the flipper. From the field profiles in the V-coil flipper we found initially that this parameter (reduced to $\lambda = 0.1$ nm) drops locally below 2. Indeed, upon raising this minimum by adding some local support field, λ_c decreased from 0.4 to 0.15 nm. In principle, a similar improvement could also be achieved by maximizing the dimensions of the flipper (if possible). Also, positioning the flipper will become less critical.

In a beam from a pulsed source (with or without choppers to further modify the pulse duration) one can use a monochromatic flipper, with good efficiency over a limited wavelength band. We give 2 examples of such flippers: flat coil and double flat coil. By proper adjustment of the current, such a flipper can be tuned to have an optimal efficiency synchronised with the neutrons of various wavelengths as they pass through the flipper. The value of this optimum depends on the wavelength range received in the detector. This range is determined by the pulse duration and the distance from the source (chopper) to the detector. For a "long duration source" and detector at small distance this means that the wavelength band in the detector will be so long that an insufficient

efficiency of the flipper results. Therefore, at such sources adiabatic flippers are preferable.

References

[1] L.W. Alvarez, F. Bloch, Phys. Rev. 57 (1940) 111.
[2] M.Th. Rekveldt, J. Phys, Colloq. C1 32 (1971) C1–579; M.Th. Rekveldt, Z. Physik 259 (1973) 391.
[3] F. Mezei, Z. Physik 255 (1972) 146.
[4] A.N. Bazhenov, et al., Nucl. Instr. and Meth. A 332 (1993) 534.
[5] G.M. Drabkin, JETP 43 (1962) 1107.
[6] T. Keller, et al., Nucl. Instr. and Meth. A 451 (2000) 474.
[7] R.T. Robiscoe, Am. J. Phys. 39 (1971) 146.
[8] W.H. Kraan, M.Th. Rekveldt, P.T. Por, Nucl. Instr. and Meth. A 300 (1991) 35.
[9] T. Takeda, H. Seto, Y. Kawabata, Appl. Phys. A 74 (Suppl.) (2002) S177.
[10] Yu.V. Taran, Dubna Report JINR P3-8577, Dubna, 1975.
[11] S.V. Grigoriev et al., Phys. Rev. A 64-1 (2001) 13614/1-11.
[12] W.H. Kraan, S.V. Grigoriev, R. Kreuger, F.M. Mulder, M.Th. Rekveldt, Physica B 297 (2001) 23.
[13] W.H. Kraan, S.V. Grigoriev, M.Th. Rekveldt, Appl. Phys. A 74 (Suppl.) (2002) S79.
[14] H. Weinfurter, G. Badurek, Nucl. Instr. and Meth. A 275 (1989) 233.
[15] B. Farago, Neutron News 12-4 (2001) 34.
[16] R. Maruyama, et al., Proceedings of PNCMI-2002, Physica B 335 (2003) 238.
[17] P.T. Por, W.H. Kraan, M.Th. Rekveldt, Nucl. Instr. and Meth. A 339 (1994) 550.
[18] A.R. Wildes, Rev. Sc. Instr. 70 (11) (1999) 4241.
[19] H. Fredrikze, R.W.E van de Kruijs, Physica B 297 (2001) 143.
[20] A.F. Schebetov, et al., Proceedings of PNCMI-2002, Physica B 335 (2003) 219.
[21] W.H. Kraan, J.B. van Tricht, M.Th. Rekveldt, Nucl. Instr. and Meth. A 276 (1989) 521.
[22] ESS Council, ESS Project Vol. I, 2002.